

# Soft Matter

Accepted Manuscript



This is an *Accepted Manuscript*, which has been through the Royal Society of Chemistry peer review process and has been accepted for publication.

*Accepted Manuscripts* are published online shortly after acceptance, before technical editing, formatting and proof reading. Using this free service, authors can make their results available to the community, in citable form, before we publish the edited article. We will replace this *Accepted Manuscript* with the edited and formatted *Advance Article* as soon as it is available.

You can find more information about *Accepted Manuscripts* in the [Information for Authors](#).

Please note that technical editing may introduce minor changes to the text and/or graphics, which may alter content. The journal's standard [Terms & Conditions](#) and the [Ethical guidelines](#) still apply. In no event shall the Royal Society of Chemistry be held responsible for any errors or omissions in this *Accepted Manuscript* or any consequences arising from the use of any information it contains.

# Pearling and arching instabilities of a granular suspension on a super-absorbing surface<sup>†</sup>

Julien Chopin,<sup>\*a</sup> and Arshad Kudrolli<sup>a</sup>

Received Xth XXXXXXXXXXXX 20XX, Accepted Xth XXXXXXXXXXXX 20XX

First published on the web Xth XXXXXXXXXXXX 200X

DOI: 10.1039/b000000x

We show that a granular suspension, composed of particles immersed in a liquid, can form pearls, hooks, and arches when deposited from a nozzle onto a translating substrate that acts as a liquid superabsorber. The removal of the liquid induces a rapid pinning of the contact line leading to mechanically stable structures that are held together by capillary adhesion with shapes that depend on the relative solidification rate. Pearls or hooks form depending on whether the suspension snaps off before or after coming in contact with the substrate. A cylindrical thread with a near circular cross-section and various undulatory structures forms if solidification occurs prior to snap-off. In particular, when the jet solidifies before coming in contact with the substrate, it folds periodically, resulting in arches with a span length determined by the deposition flux and the substrate speed. Period doubling and meandering are observed to lead to further structures with vertical and horizontal ripples when the deposition flux is increased.

## 1 Introduction

The process by which a liquid drop or jet impacting on a surface undergo solidification is important in many natural processes and technological applications as in the formation of ice and lava stalagmites, thermal spray coating<sup>1</sup>, inkjet printing<sup>2</sup>, and 3D writing<sup>3–5</sup>. While significant fundamental research has focused on the hydrodynamic instabilities of a homogeneous fluid experiencing dripping<sup>6</sup>, splashing<sup>7,8</sup>, and dewetting<sup>9</sup>, the understanding of the coupling between the flow dynamics and solidification is still in its infancy. In particular, most experiments and simulations are in a regime of slow solidification (that may further include a phase transition or chemical reaction) which only results in a perturbation of the spreading dynamics on a surface<sup>10,11</sup>.

Recently, we demonstrated that a granular suspension dripped onto a substrate leads to growth of intricate tower structures that are held together by capillary cohesion<sup>12</sup>. The necessary condition was that the substrate acts as a superabsorber for the liquid in the suspension. Here, we show that such a rapid solidification coupled with instabilities (Rayleigh-Plateau or jet breakup, stick-slip contact line dynamics, etc.) can lead to novel compact and undulatory structures on a superabsorbing surface which is translating horizontally. The translation rate gives rise to a further time scale which is important to the formation of the observed structures.

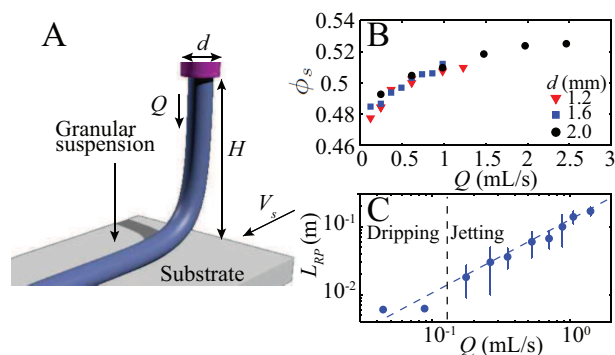


**Fig. 1** (A) A schematic of a granular suspension emerging from a nozzle with a flux  $Q$  and falling as a uniform thread onto a substrate translating with a speed  $V_s$ . (B) The solid volume fraction  $\phi_s$  of the suspension emerging from the nozzle is observed to increase with  $Q$  and is essentially independent of nozzle diameter  $d$ . (C) The jet length  $L_{RP}$  before it breaks up into droplets due to a Rayleigh-Plateau-like instability is observed to increase linearly with  $Q$  in the jetting regime. The transition from dripping to jetting occurs at  $Q \sim 0.15$  mL/s.

<sup>†</sup> Electronic Supplementary Information (ESI) available: See DOI: 10.1039/b000000x/

<sup>a</sup> Department of Physics, Clark University, Worcester, MA 01610 USA. E-mail: jchopin@clarku.edu; akudrolli@clarku.edu

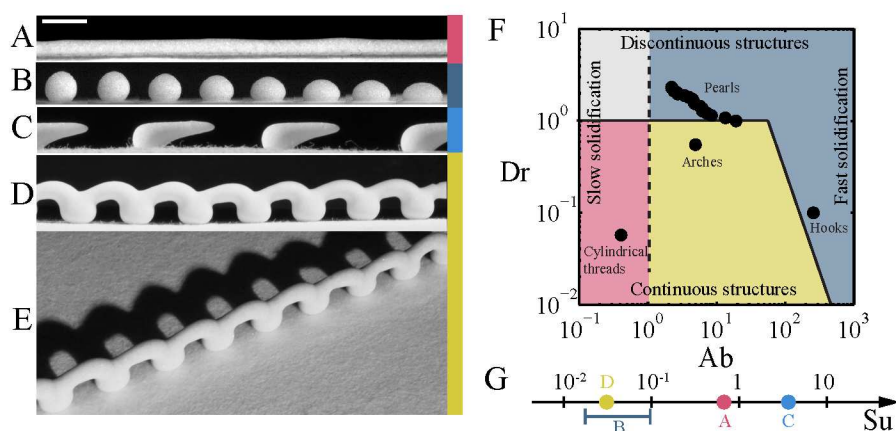


**Fig. 2** Examples of solidified structures obtained due to pearling and arching instabilities. (A) A cylindrical thread corresponding to the base state of the system is observed when arching and pearling instabilities do not have time to develop before solidification ( $d = 2.0$  mm,  $Q = 0.35$  mL/s,  $V_s = 9.7$  cm/s). (B) Spherical to oblate axisymmetric pearls form in the dripping regime when  $H$  is varied linearly from 6 mm to 14 mm from left to right ( $d = 1.2$  mm,  $Q = 0.044$  mL/s). (C) Hook shapes are obtained when the snap off occurs after the drop has contacted the superabsorbing substrate and solidification has reached the bridge connecting the drop and the nozzle ( $d = 2.0$  mm,  $Q = 0.18$  mL/s,  $V_s = 2.4$  cm/s,  $H = 2.5$  mm). (D) Periodic arches are observed when the solidification rises up the thread in the jetting regime which folds because of gravity and solidifies ( $d = 2.0$  mm,  $Q = 0.18$  mL/s,  $V_s = 1.2$  cm/s,  $H = 10$  mm). (E) The same arches viewed in perspective illustrate their 3D nature. Scale bar is 4 mm. (F) Phase diagram in the  $Ab$ - $Dr$  plane showing four different regimes depending on the relative solidification rate ( $Ab > 1$  and  $Ab < 1$ ) and flow regime (jetting and dripping).  $Ab$  and  $Dr$  are the absorption and dripping numbers respectively (see text for their definitions). Black disks correspond to the experimental data shown in A to E. (G) The same data are organized along the  $Su$ -axis highlighting, in particular, that hooks forms at high substrate speed ( $Su \gg 1$ ).  $Su$  is the dimensionless substrate speed (see text for its definition)

In contrast with intricate weaving patterns observed with a Newtonian fluid<sup>13–15</sup>, we show that the observed structures which include pearls, hooks, and arches are not only three dimensional and mechanically stable, but also have a different physical origin because of rapid solidification. In addition to finding novel coupling between solidification and hydrodynamical instabilities, our work can be viewed as providing an alternative strategy to wet granulation and moulding to deliver and shape amorphous powders. A significant advantage is that the powder can be suspended and transported in a liquid medium under ambient temperature, which can be drawn away, as the desired form is attained.

## 2 Experiment

A schematic of the experimental system along with the control parameters is shown in figure 1 A. A nozzle with diameter  $d$  attached to a pump syringe is located at height  $H$  vertically above a substrate which is mounted on a horizontal translating stage driven by a stepper motor. Nozzles with inner diameter of  $d = 1.2$ , 1.6, and 2.0 mm are used. The substrate speed  $V_s$  is varied between 1 and 20 cm/s. Unless otherwise stated, a blotting paper is used as the liquid absorbing substrate with the absorption strength characterized by liquid absorption co-

efficient in the medium  $D = 4 \times 10^{-6}$  m<sup>2</sup>/s (figure S1) (see online supplementary materials). The substrate needs to have a sufficiently high absorption strength for fast drainage and solidification and is thus called superabsorber.

The granular suspension used consists of glass beads with radius  $a = 17 \pm 10 \mu\text{m}$  immersed in water with a viscosity  $\mu = 0.9$  mPa·s and surface tension  $\gamma \approx 70$  mN/m<sup>2</sup>. A suspension is prepared by first pouring 30 mL of liquid in a 60 mL syringe and then filling it with the glass beads which sediment to the bottom. A stepper motor is used to control  $Q$  over the range 0.01 – 2.0 mL/s. The volume fraction of the glass beads in the suspension  $\phi_s$  which emerges from the nozzle is seen to increase slowly with  $Q$  as shown in figure 1 B (see online supplementary materials for methods). This trend shows that the liquid entrains more grains with  $Q$  as it moves through the sedimented bed inside the syringe. We also find that the granular suspension transitions from emerging as a drop to a jet near the nozzle at  $Q \sim 0.15$  mL/s. However, because a uniform jet will eventually break-up into drops because of a Rayleigh-Plateau-like instability<sup>16</sup>, we measure the distance the suspension falls  $L_{RP}$  during that time in figure 1 C. Thus, by using an appropriate  $H$ , one can choose whether the suspension impacts the substrate as a drop or as a continuous jet.

Examples of the structures obtained depending on the various instabilities and their sequence relative to solidification are

shown in figure 2 and movies S1 to S4. In the jetting regime and for  $H < L_{RP}$ , we find a continuous cylindrical thread as shown in figure 2 A and movie S2 at relatively high  $V_s$  and  $Q$ . This uniform thread is measured to have a large contact angle with the substrate ( $\theta_c \approx 140$  deg.) and may be considered as the base state of the system. By choosing  $Q$  in the dripping regime, we find that a spherical or oblate pearl forms depending on  $H$  (see figure 2 B and movie S3). Hooks are obtained when the snap off and solidification occur well after the suspension comes in contact with the substrate (see figure 1 C and movie S4). The effect of solidification is even more dramatic at smaller substrate speed when we observe the spontaneous emergence of arches with periodic contact with the substrate as the contact line performs stick-slip motion (see figure 1 D and movie S1).

These structures are fully self-supporting as seen in figure 1 E. It may be noted that they are held together by the cohesive forces which arise in the residual liquid which remain between the grains in the suspension. In the laboratory, we have found the reported structures survive for days if not months as the residual liquid evaporates and develops weak Si - O - Si bonds<sup>17</sup>. Addition of binders in the suspending liquid phase for example can enhance the binding strength between grains after the residual liquid evaporates allowing structures to be assembled from amorphous solids. However, this is not a focus of the study here, and we do not discuss it further.

In order to understand the relative importance of the main control parameters in our experiments, we introduce a dimensionless substrate speed  $Su = V_s/V_{fl}$ , which corresponds to the ratio of the substrate speed  $V_s$  and the flow speed of the suspension out of the nozzle  $V_{fl}$  given by  $4Q/(\pi d^2)$  in the jetting regime and by the impact velocity  $V_i$  in the dripping regime. Further, we introduce a second dimensionless number, the dripping number  $Dr = H/L_{RP}$ , where  $Dr > 1$  corresponds to the dripping regime, and  $Dr < 1$  corresponds to the jetting regime. With this definition, it appears as if  $Dr$  is independent of  $V_s$  because  $L_{RP}$  is measured here without a substrate. However, this is not true when the suspension falls on to a substrate in the regime where  $Dr$  is small and  $V_s$  is large, because the contact with the substrate due to its relative motion results in dragging and stretching of the liquid jet before it freezes or snaps off. As, we will see later, this additional dynamics plays an important role in the formation of the structures observed in this regime. Finally, we introduce a third dimensionless number  $Ab = \tau_S/\tau_D$  which is the ratio of the spreading timescale  $\tau_S$  and drainage timescale  $\tau_D$ . When  $Ab = 0$ , the suspension spreads like an effective viscous fluid without solidification. When  $Ab \gg 0$ , the suspension solidifies with little spreading.

We now discuss how the three non-dimensional parameters  $Su$ ,  $Dr$ , and  $Ab$  allow us to organize a phase diagram of the various observed structures. To aid visualization, we plot the

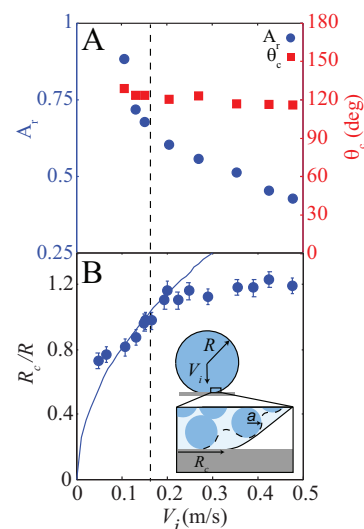


**Fig. 3** Illustration of the effect of solidification on the equilibrium shape of a pearl. (A) The aspect ratio  $A_r$  of a pearl is observed to decrease with  $V_i$  while the contact angle with the substrate  $\theta_c$  is roughly constant and is surprisingly high for a water-based suspension spreading on a hydrophilic substrate. These shapes illustrate the strong effect of solidification. The experimental parameters are the same as in figure 2 B. (B) The normalized contact radius  $R_c/R$  as a function of  $V_i$  is fitted using Eq. 1 below  $V_i = 0.16$  cm/s (blue line) with  $\tau_D = 7.2$  ms. Inset: Schematics of a drop upon impact with a close-up of the contact line.

projection of the 3D phase diagram in the plane  $Ab$ - $Dr$  (figure 1 F) and along the line  $Su$  (figure 1 G). In the  $Ab$ - $Dr$  plane, four regions are identified. Cylindrical threads are obtained for  $Ab < 1$ , i.e. relatively slow solidification rate. Pearls, hooks and arches are obtained for  $Ab > 1$ . Interestingly, discontinuous structures (hooks) can be obtained when  $Dr < 1$  but for large  $Ab$  and  $Su$ . Indeed, the jet is dragged by the substrate in the hook regime (due to small  $H$  or  $Dr < 1$ ) stretching it and ultimately leading the jet to snap off, when  $Su \gg 1$ .

### 3 Pearling

To understand the process by which these structures form, we next examine their physical features and the conditions under which they occur, in more detail. In particular, we provide the scalings for the three dimensionless numbers allowing us to add experimental data on the phase diagram. Figure 3 A shows a plot of the height to width aspect ratio  $A_r$  of the pearls to capture the degree of sphericity along with the contact angle with the substrate  $\theta_c$  as a function of impact speed  $V_i$ . While  $A_r \sim 1$  for low  $V_i$  and then decreases,  $\theta_c$  remains obtuse and roughly constant over the larger range of  $V_i$ . These shapes are thus reminiscent of liquid drops sitting on a hydrophobic

substrate, which may appear surprising given the hydrophilic nature of the superabsorbing surface. However, we can understand these shapes by the fact that the solidification rapidly pins the contact line (CL) when a small volume of liquid is drained near the CL, leading to a rough air/liquid/grain interface as illustrated in the inset to figure 3 B. Such an interface causes a yield stress to develop because of the capillary cohesion and friction between particles at the surface<sup>12</sup>.

We plot the measured radius of the contact area  $R_c$  scaled by the radius  $R$  of the drop prior to contact as a function of  $V_i$  in figure 3 B.  $R_c/R$  appears to have a finite value at low  $V_i$  and grows nonlinearly before appearing to plateau at higher  $V_i$ . This trend can be understood from the fact that a certain time is required for the excess liquid to drain, which will yield a very small contact area when the impact speed is small. However, as  $V_i$  increases the contact area can be expected to grow because greater kinetic energy is available to overcome viscous dissipation of the drop before it solidifies. We therefore consider the characteristic timescale  $\tau_D$  for the drainage of a thin liquid layer of thickness  $\xi$  after the suspension first comes in contact with the substrate. Over this time, the drop spreads on the substrate and forms a contact area with radius given by :

$$R_c/R \sim \sqrt{\tau_D V_i / R}. \quad (1)$$

This estimate is obtained using a simple geometric argument which assumes a spherical drop and is thus valid for small deformations ( $R_c/R \ll 1$ ), *i.e.* for times shorter than the impact duration  $\tau_i \sim R/V_i$ . Forcing a fit of the experimental data for  $V_i < 0.16$  m/s (corresponding to  $\tau_i > 7.5$  ms) with  $\tau_D$  as the adjustable parameter, we find  $\tau_D = 7.2$  ms. Further, using an imbibition mechanism,  $\tau_D$ ,  $D$ , and  $\xi$  are found to be linked by the dimensional relation

$$\tau_D \sim \xi^2 / D \quad (2)$$

We are unable to measure  $\xi$  directly, but we can estimate it from the solid volume fraction both before and after impact,  $\phi_s \approx 50\%$  and  $\phi_s^* \approx 63\%$ , respectively. Hence,  $\xi \approx (R/3)(\phi_s^* - \phi_s)/\phi_s \sim 100 \mu\text{m}$ . Thus, our model gives  $\tau_D \sim 2.5$  ms which is of the same order of magnitude as previously estimated. Using this model, we can give a scaling for the various dimensionless numbers. In the pearling regime, we have  $Ab \sim RD/(V_i \xi^2)$ , assuming that  $\tau_s \sim \tau_i$  and  $Su \sim V_s/V_i$  where we used the fact that  $V_{fl} \sim V_i$ . Using experimental data from figure 2, we obtain  $Ab$  in the range 0.5-20 and  $Su$  in the range 0.02-0.1. Overall, we find that at small impact speed, drainage is faster than the impact ( $Ab > 1$ ), which results in pearls that are solidified in a configuration, far from equilibrium.

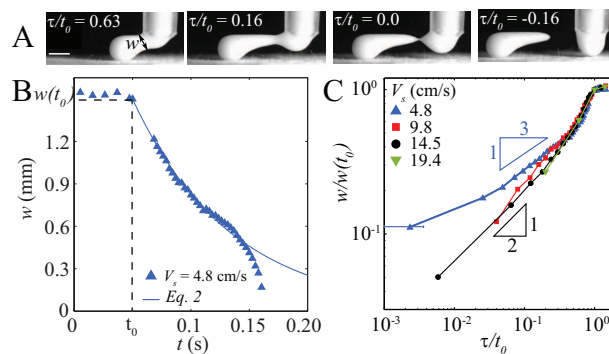


**Fig. 4** Hook formation and anomalous pinch off dynamics of a stretched solidifying liquid bridge. (A) Sequence of hook formation (thick blotter,  $d = 2.0$  mm,  $Q = 0.088$  mL/s,  $V_s = 4.8$  cm/s,  $H = 2.5$  mm). Scale bar is 2 mm. (B) Temporal evolution of the liquid bridge waist  $w$  where an exponential thinning is observed. From a fit of the data (solid line), we measure  $\zeta \approx 2.7$  mm. (C)  $w/w(t_0)$  as a function of the normalized time to breakup  $\tau/t_0$  for a fixed flux  $Q = 0.88$  mL/s and varying  $V_s$ . For high substrate speed, the diameter follows the scaling  $w \sim t^\alpha$  with ( $\alpha = 0.53 \pm 0.05$ ) while a qualitatively different dynamics is observed at lower substrate speed ( $V_s = 4.8$  cm/s) with ( $\alpha = 0.35 \pm 0.05$ ).

## 4 Hook formation

We next discuss the hooks which form when a snap off occurs after the drop comes in contact with the substrate as shown in the sequence of images in figure 4 A and movie S4. This occurs for small  $Dr$  ( $< 1$ ) and large  $Su$  (in the range 5-50). The solid phase can be noted to first grow off the substrate and the liquid thread is stretched. After snap off, the tips recede somewhat on the side attached to the substrate, and fully on the side attached to the nozzle. Figure 4 B shows the minimal waist of the liquid thread  $w$ . For  $t > t_0$  set by the substrate speed, we use a function typically used to describe the waist of a liquid bridge undergoing pinch off<sup>18</sup>

$$w(t) = w(t_0) \exp(-V_s(t - t_0)/2\zeta), \quad (3)$$

with  $\zeta$  as a fitting parameter. An exponential fit is observed for several  $V_s$  with  $\zeta \approx 2.7$  mm which is the typical length of the liquid thread. Due to its kinematic origin, the decrease of the waist is essentially independent of the fluid rheology. Then, for small waist ( $w \sim 0.6$  mm) capillary effects become dominant resulting in an accelerated thinning of the thread until snap off occurs at time  $t_b$ . In Figure 4 C, we plot in log-log  $w/w(t_0)$  as a function of  $\tau/t_0$  varying the substrate speed, where  $\tau = t_b - t$  is the time from breakup. The minimal waist is found to scale as  $(\tau/t_0)^\alpha$  with an exponent  $\alpha$  that depends on the substrate speed. At high speed ( $V_s \geq 9.8$  cm/s), we measure  $\alpha = 0.53 \pm 0.05$  which is clearly different from Newtonian fluids ( $\alpha = 1$ )<sup>19</sup> and smaller than observed previously

with dense suspensions ( $\alpha = 2/3$ )<sup>20</sup>. A still smaller exponent ( $\alpha = 0.35 \pm 0.05$ ) is measured at smaller speed ( $V_s = 4.8$  cm/s) which may be due to the fact that the suspension is on the verge of solidification at snap off.

## 5 Arching

When  $V_s$  is lowered further, pinch off does not occur and a continuous thread falls on and off the substrate resulting in arches (figure 2 G and movie S1). This occurs because the solidification rate of the thread up off the substrate slows down with height, and the fluid region of the thread falls back on the substrate because of gravity, which then quickly solidifies upon contact in the shape of an arch. This process then repeats itself giving rise to various undulatory structures besides arches. In figure 5 A, B, and C, we show the structures obtained by increasing the suspension flux while keeping  $V_s$  constant. At low flux, slender arches are obtained. When the flux is increased, due to volume conservation, the arches are thicker and thus the undulations appear with smaller amplitudes and resemble ripples. The key difference is that the solidification front rises up the jet in case of arches, whereas solidification occurs after the jet comes in contact with the substrate in case of ripples. This fact can be seen from the bright spot in the images (figure 5 A, B, and C), which indicates the presence of a thin superficial liquid layer reflecting light.

Further, as  $Q$  is increased, period doubling can lead to superposition of ripples and arches (see movie S5), and at still larger  $Q$ , the structure is decorated by ripples that oscillates sideways (see movie S6). Although this meandering instability is reminiscent of the coiling of a purely viscous jet on a translating substrate<sup>13</sup>, the mechanism is different here because it does not rely on a viscous buckling instability, but rather on the pinning of the contact line and solidification.

The undulating structures can be characterized quantitatively by measuring the span and base lengths,  $l_s$  and  $l_b$ , respectively. We find that  $l_s$  reaches a maximum with respect to  $Q$  (figure 5D) and  $V_s$  (figure 5E) while  $l_b$  is approximately  $Q$ -independent and increases continuously with  $V_s$ . Therefore a specific combination of flow rate and substrate speed results in an optimal span length. This optimal length can be understood from the tower growth model<sup>12</sup> and the CL pinning introduced in the discussion on the drop impact analysis earlier. Arches can be thought to develop as leaning towers growing with an angle  $\alpha$  with respect to the substrate (see figure 5A) reaching their maximum height  $h_X$  before falling. Thus,  $h_X \sim \Phi D / v_G$ , where  $v_G = (\phi / \phi^*) Q / s$  is the growth velocity,  $s$  the arch cross section,  $\Phi = \phi_s / (\phi_s^* - \phi_s)$ , and  $\phi_s^*$  the solid volume fraction after solidification.  $v_G$  is of the order of 20 cm/s and always smaller than  $V_s$ . The arch span length is then defined as the projected height on the substrate  $l_s \sim h_X \cos \alpha$  where  $\cos \alpha \approx V_s / v_g$  (for  $V_s \ll v_G$ ) yielding  $l_s \sim \Phi D V_s / v_G^2$ . This

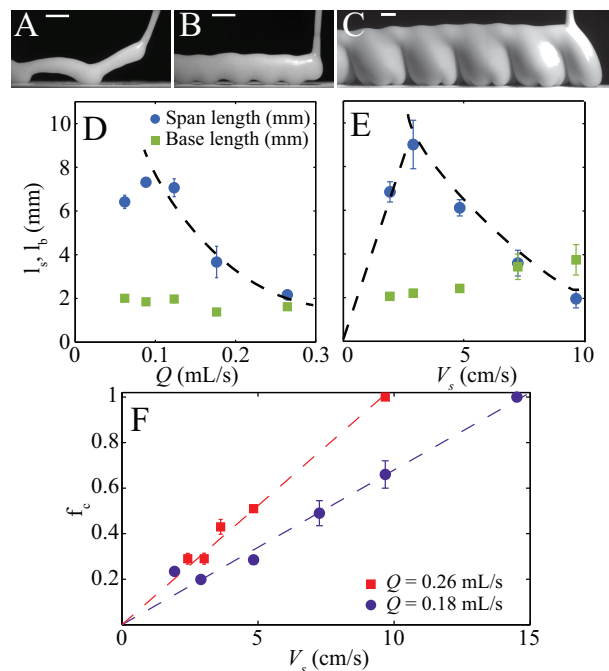


**Fig. 5** Images of undulating structures obtained by increasing the flux  $Q$  including (A) arches (thin blotter,  $Q = 0.12$  mL/s,  $V_s = 2.4$  cm/s,  $d = 1.19$  mm), (B) ripples (thin blotter,  $Q = 0.26$  mL/s,  $V_s = 2.4$  cm/s,  $d = 1.19$  mm) and (C) meandering bumps (thick blotter,  $Q = 1.76$  mL/s,  $V_s = 1.2$  cm/s,  $d = 2.0$  mm). Arches are characterized by the span distance and a base length. Scale bars are 4 mm. (D) Evolution of the span (green squares) and base length (blue disks) with the flow rate at  $V_s = 2.4$  cm/s. A sharp decrease of the spacing is observed for  $Q \sim 0.15$  mL/s separating the arch mode with the ripple mode. (E) Base and span lengths as a function of the substrate speed  $V_s$  at  $Q = 0.18$  mL/s. (F) Evolution of the fractional contact length  $f_c$  with  $V_s$  for two flow rates  $Q = 0.18$  mL/s and  $Q = 0.26$  mL/s showing a linear increase.

law captures qualitatively the decrease with  $Q$  and the increase with  $V_s$  at small substrate speed. The maximum observed with  $Q$  may be attributed to the influence of the nozzle which constrains the tower height. This constraint is observed at small  $Q$ , because  $H$  has to be decreased accordingly to avoid dripping.

Next, to understand the decrease of  $l_s$  with  $V_s$  at higher substrate speed, we measure the fractional contact length defined as  $f_c = l_b/(l_s + l_b)$  ( $0 < f_c \leq 1$ ) for different flow rates by varying the substrate speed (figure 5F).  $f_c$  is found to increase linearly with the substrate speed until the arch instability is completely suppressed ( $f_c = 1$ ) which occurs at  $V_s = 14.6\text{cm/s}$  for  $Q = 0.18\text{mL/s}$  and  $V_s = 9.5\text{cm/s}$  at  $Q = 0.26\text{mL/s}$ . The shape obtained is thus a cylindrical thread in constant contact with the substrate along its length. In this regime, the CL speed is simply  $V_s$  and the characteristic time for spreading is then  $\tau_S \sim \xi/V_s$  which is the time to renew a volume of typical size  $\xi$  near the CL. Solidification is not fast enough to pin the contact line when  $\tau_S \sim \tau_D$ , yielding a crossover speed  $V_s^X \sim D/\xi \sim 2\text{cm/s}$  which corresponds to the maximum observed in figure 5D. When  $V_s > V_s^X$ , the thread falling back on the substrate experiences an extended spreading before being pinned resulting in larger  $l_b$  and smaller  $l_s$  due to a comparatively slow solidification rate.

We can now give the scaling for  $Ab$  in the cylindrical and arch regime. Using equation 2 and  $\tau_S \sim \xi/V_s$ , we obtain  $Ab \sim D/(V_s \xi)$  which is  $\sim 0.4$  in the cylindrical regime and  $\sim 4$  in the arch regime. However, the formation of arch involves periodic impacts of the thread on the substrate, therefore,  $Ab$  is best estimated using the scaling of the pearl regime, yielding  $Ab$  in the range  $5 - 10^2$  depending on the impact speed which can vary from 1 to  $30\text{cm/s}$ .

## 6 Conclusions and Perspectives

In conclusion, we have shown that a new class of structures arise in rapidly solidifying flows driven by a rapid removal of a liquid from a dense suspension as it comes into contact with a liquid superabsorber along with other dynamical instabilities. These structures go well beyond the vertical slender tower structures, we have demonstrated previously<sup>12</sup>, which arise when a granular suspension is dripped onto a stationary substrate. We find that a variety of shapes including spherical and oblate pearls, arches, and hooks can spontaneously form depending on the liquid absorption rate, the degree of spreading, flux, and substrate speed.

Accordingly, we introduce three dimensionless numbers  $Su$ ,  $Dr$ , and  $Ab$ , which capture the ratio of the substrate and flux velocity, the drop height relative to the length of the emerging jet before breaks up, and spreading and absorption time scales, respectively to organize a phase diagram covering the various regimes investigated. Using these three dimen-

sionless numbers, one can understand the overall features observed in the phase diagram and the conditions under which they occur. In particular, when  $Ab > 1$ , pearls occurs for  $Dr > 1$  and hooks for  $Dr < 1$  and large  $Su$ . At moderate  $Su$  and  $Dr < 1$ , arches are obtained. For smaller  $Ab (< 1)$ , the observed structures are the cylindrical threads.

Further, unlike a viscous Newtonian fluid which gives rise to various meandering patterns in a thin horizontal layer which is in contact with the substrate, and thus essentially two dimensional<sup>13–15</sup>, the structures obtained are three dimensional. Because of the paramount importance of liquid absorption and solidification, the origin of the structures is also quite different from that for a viscous thread interacting with a substrate where gravity and viscous forces set the length and time scales relative to translation. Thus, the spreading dynamics where the flow over the substrate is coupled with a solidifying process yields a rich set of patterns which underlies a complex non-linear dynamical system. In this context, it would be interesting to consider how one can move from one limit to the other by changing the viscosity of the suspending fluid which will progressively reduce drainage rate but introduce viscous force. However, this is beyond the scope of this investigation.

Finally, our study offers not only an opportunity to develop granular suspension models which undergo rapid jamming, but also applications as noted in the introduction. Specifically, current 3D printer matrices rely on using a temporary filling which need to be dissolved away to create an arch or dome like structure. This is not only cumbersome but also not feasible when a hole is desired which cannot be reached after assembly of the structure. The demonstration of the formation of arches, besides other rich variety of structures, suggests the potential of granular suspension and our technique towards such applications.

## Acknowledgments

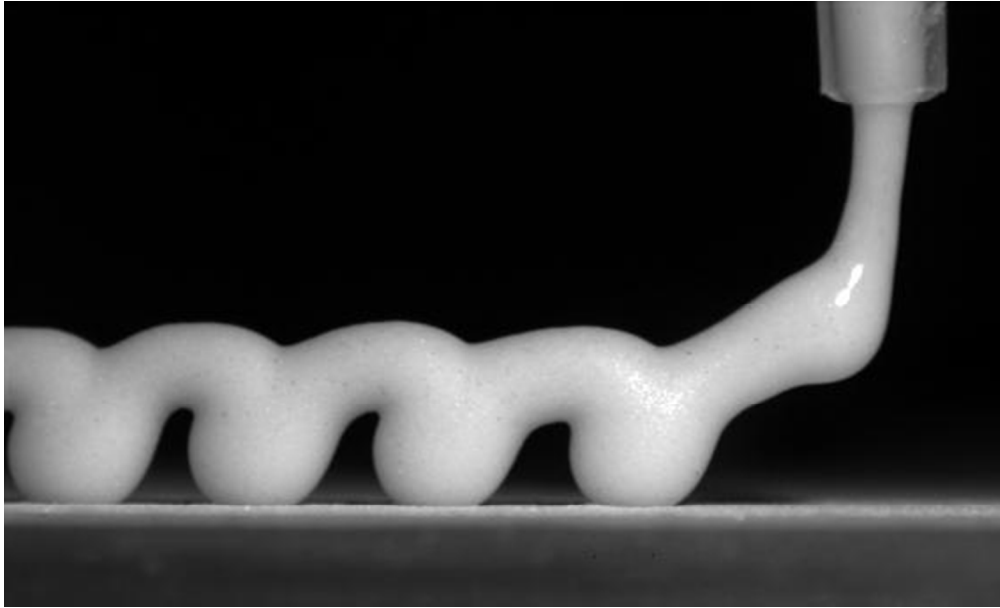
We thank Pascal Jundt and Suyesh Thapa for their help with experiments.

## References

- 1 P. Fauchais, A. Vardelle, M. Vardelle and M. Fukumoto, *J. Therm. Spray Technol.*, 2004, **13**, 337–360.
- 2 P. Calvert, *Chem. Mater.*, 2001, **13**, 3299.
- 3 F. Gao and A. A. Sonin, *Proc. R. Soc. London Ser. A*, 1994, **444**, 533–554.
- 4 J. A. Lewis, *Adv. Funct. Mater.*, 2006, **16**, 2193–2204.
- 5 Y. Gao, H. Li and J. Liu, *PLOS ONE*, 2012, **7**, e45485.
- 6 J. Eggers and E. Villermaux, *Rep. Prog. Phys.*, 2008, **71**, 036601.
- 7 A. L. Yarin, *Annu. Rev. Fluid Mech.*, 2006, **38**, 159.
- 8 L. A. Lubbers, Q. Xu, S. Wilken, W. W. Zhang and H. M. Jaeger, *Phys. Rev. Lett.*, 2014, **113**, 044502.
- 9 R. Craster and O. Matar, *Rev. Mod. Phys.*, 2009, **81**, 1131.
- 10 M. Pasandideh-Fard, S. Chandra and J. Mostaghimi, *Int. J. Heat Mass Transfer*, 2002, **45**, 2229–2242.

- 
- 11 Q. Xu, E. Brown and H. M. Jaeger, *Phys. Rev. E*, 2013, **87**, 043012.
  - 12 J. Chopin and A. Kudrolli, *Phys. Rev. Lett.*, 2011, **107**, 208304.
  - 13 S. Chiu-Webster and J. R. Lister, *J. Fluid Mech.*, 2006, **569**, 89–112.
  - 14 S. W. Morris, J. H. Dawes, N. M. Ribe and J. R. Lister, *Phys. Rev. E*, 2008, **77**, 066218.
  - 15 P. Brun, N. Ribe and B. Audoly, *Phys. Fluids*, 2012, **24**, 043102.
  - 16 C. Bonnoit, T. Darnige, E. Clément and A. Lindner, *J. Rheol.*, 2010, **54**, 65.
  - 17 N. Olivi-Tran, N. Fraysse, P. Girard, M. Ramonda and D. Chatain, *The European Physical Journal B - Condensed Matter and Complex Systems*, 2002, **25**, 217–222.
  - 18 G. H. McKinley and T. Sridhar, *Annu. Rev. Fluid Mech.*, 2002, **34**, 375–415.
  - 19 J. Eggers, *Rev. Mod. Phys.*, 1997, **69**, 865.
  - 20 M. Miskin and H. Jaeger, *Proc. Natl. Acad. Sci. U.S.A.*, 2012, **109**, 4389.





Spontaneous formation of arches when a granular suspension is deposited on a translating substrate composed of dry granular beads which acts as superabsorber for the interstitial fluid.  
200x121mm (72 x 72 DPI)

Textual abstract

Arches, hooks, and pearls are observed to spontaneously assemble when a granular suspension is dripped onto a moving liquid-absorbing substrate.